11-2015

Measurement of interaction between antiprotons

Adam Gibson-Even
Valparaiso University

Shirvel Stanislaus
Valparaiso University

Donald Koetke
Valparaiso University

STAR Collaboration

LETTER

doi:10.1038/nature15724

Measurement of interaction between antiprotons

The STAR Collaboration*

One of the primary goals of nuclear physics is to understand the force between nucleons, which is a necessary step for understanding the structure of nuclei and how nuclei interact with each other. Rutherford discovered the atomic nucleus in 1911, and the large body of knowledge about the nuclear force that has since been acquired was derived from studies made on nucleons or nuclei. Although antinuclei up to antihelium-4 have been discovered[1] and their masses measured, little is known directly about the nuclear force between antinucleons. Here, we study antiproton pair correlations among data collected by the STAR experiment[2] at the Relativistic Heavy Ion Collider (RHIC)[3], where gold ions are collided with a centre-of-mass energy of 200 gigaelectronvolts per nucleon pair. Antiprotons are abundantly produced in such collisions, thus making it feasible to study details of the antiproton–antiproton interaction. By applying a technique similar to Hanbury Brown and Twiss intensity interferometry[4], we show that the force between two antiprotons is attractive. In addition, we report two key parameters that characterize the corresponding strong interaction: the scattering length and the effective range of the interaction. Our measured parameters are consistent within errors with the corresponding values for proton–proton interactions. Our results provide direct information on the interaction between two antiprotons, one of the simplest systems of antinucleons, and so are fundamental to understanding the structure of more-complex antinuclei and their properties.

Although the theory of quantum chromodynamics (QCD) provides us with an understanding of the foundation of the nuclear force, this binding interaction in nuclei operates at low energy, where the force is strong and difficult to calculate directly from the theory (see ref. 5 and references therein for recent developments). For that reason, a common parameterization of the effective interaction between nucleons is based on experimental measurements, and the corresponding parameterization for antinucleons remains undetermined. The important paramfeters in such a description of the interaction are the scattering length (f_0), which is related to elastic cross-sections, and the effective range of the interaction (d_0), which is determined to be a few femtometres (the typical nuclear scale). For a short range potential, these two parameters are related to the s-wave scattering phase shift δ_0 and the collision momentum k by $k\cot(\delta_0) \approx \frac{1}{f_0} + \frac{1}{2}d_0k^2$. The existence and production rates of antinuclei offer indirect information about interactions between antinucleons, and also have relevance to the unexplained baryon asymmetry in the Universe[6]. Antinuclei produced to date include antiprotons, antideuterons, antitritons, antihelium-3, and the recently discovered antihypertriton and antihelium-4 (see ref. 1 and references therein). The interaction between two antinucleons is the basic interaction that binds the antinucleons into antinuclei, and this has not been directly measured previously. Of equal importance, one aspect of the current measurement is a test of matter–antimatter symmetry, more formally known as CPT—a fundamental symmetry of physical laws under the simultaneous transformations of charge conjugation (C), parity transformation (P) and time reversal (T). Although various prior CPT tests[7] have been many orders of magnitude more precise than what is reported here, there is value in independently verifying each distinct prediction of CPT symmetry[7].

Ultra-relativistic nuclear collisions produce an energy density similar to that of the Universe microseconds after the Big Bang, and the high energy density creates a favourable environment for antimatter production. The abundantly produced antiprotons provide the opportunity to measure, for the first time, the parameters f_0 and d_0 of the strong nuclear force between antinucleons rather than nucleons.

The technique used to probe the antiproton–antiproton interaction involves momentum correlations, and it resembles the space-time correlation technique used in HBT (Hanbury Brown and Twiss) intensity interferometry. Since its invention for use in astronomy in the 1950s[4], the HBT technique has been adopted in many areas of physics, including the study of the quantum state of Bose–Einstein condensates[8], and the correlation among electrons[9] and among atoms in cold Fermi gases[10]. A Bose–Einstein enhancement in particle physics was first observed in the late 1950s as an enhanced number of pairs of identical pions produced with small opening angles, the GGLP (Goldhaber, Goldhaber, Lee and Pais) effect[11]. Later on, Kopylov and Podgoretsky noted the common quantum statistics origin of the HBT and GGLP effects[12], and, through a series of papers (see a review[13] and references therein), they devised the basics of the momentum correlation interferometry technique. In this technique, they introduced the correlation functions (CFs) as ratios of the momentum distributions of correlated and uncorrelated particles, $C(\boldsymbol{p}_1, \boldsymbol{p}_2) = \frac{P(\boldsymbol{p}_1, \boldsymbol{p}_2)}{P(\boldsymbol{p}_1)P(\boldsymbol{p}_2)}$ with $C = 1$ for no correlations, suggested the so-called mixing technique to construct the uncorrelated distribution by using particles from different collisions (events), and formulated a simple relation of the CFs with the space-time structure of the particle emission region. Here $C(\boldsymbol{p}_1, \boldsymbol{p}_2)$ is the correlation function, $P(\boldsymbol{p}_1)$ and $P(\boldsymbol{p}_2)$ are probabilities for detecting a particle with momentum $\boldsymbol{p}_1$ and a particle with momentum $\boldsymbol{p}_2$, respectively, and $P(\boldsymbol{p}_1, \boldsymbol{p}_2)$ is the joint probability for detecting both simultaneously. As a result, the momentum correlation technique has been widely embraced by the nuclear physics community[14–17].

Figure 1 illustrates the process of constructing two-particle correlations in heavy-ion collisions. In addition to quantum statistics effects, final state interactions (FSIs) play an important role in the formation of correlations between particles. FSIs include, but are not limited to, the formation of resonances, the Coulomb repulsion effect, and the nuclear interactions between two particles[14,15,18,19]. In fact, FSI effects provide valuable additional information. They allow for (see refs 16, 20 and references therein) coalescence femtoscopy, correlation femtoscopy with non-identical particles, including access to the relative space-time production asymmetries, and a measurement of the strong interaction between specific particles. The last measurement is often difficult to access by other means and is the focus of this paper (for recent studies see refs 21, 22).

In a semi-classical geometrical description, a complex heavy-ion collision can be regarded as a superposition of many individual nucleon–nucleon collisions, each governed by a constant probability of interaction with all nucleons travelling in straight lines. The centrality corresponds to the extent that two nuclei overlap, and events are categorized by their

*Lists of participants and their affiliations appear at the end of the paper.

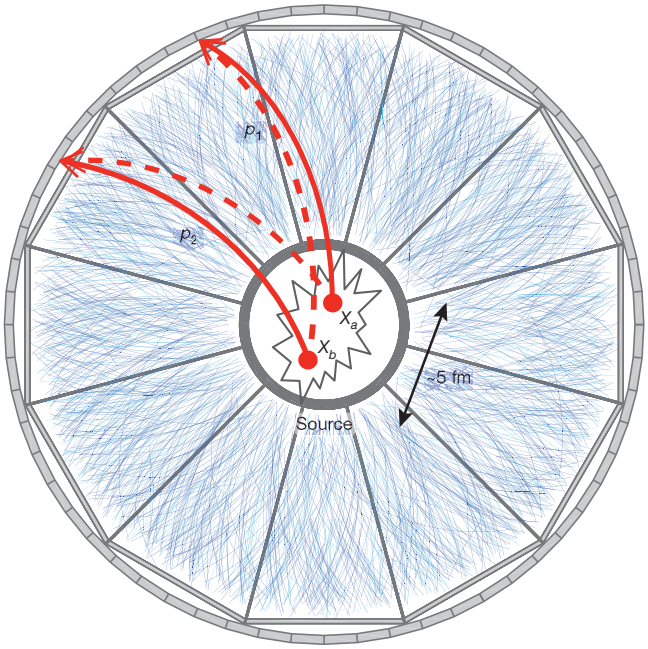

Figure 1 | A schematic of the two-particle correlation process in a heavy-ion collision. The display is overlaid on an event display from the Time Projection Chamber in the STAR detector. The curves show particle trajectories, from which the track momenta are determined. These trajectories are measured in three dimensions, but are projected onto a single plane in this illustration. The STAR detector measures three-vector momenta over a wide range beginning at about 0.1 GeV c^{-1}. Two particles emitted from two separated points, with four-coordinates X_a and X_b, are detected with four-momenta p_1 and p_2. For the pair of indistinguishable particles with even/odd total spin, the two quantum mechanical amplitudes (representing, for non-interacting particles, products of plane waves $\langle p_1|X_a\rangle \langle p_2|X_b\rangle$ and $\langle p_2|X_a\rangle \langle p_1|X_b\rangle$, where $\langle p|X\rangle = \exp(-ipX)$) must be added/subtracted to yield the amplitude which is symmetric/antisymmetric with respect to the interchange of particle momenta. This results in an enhancement/suppression in the joint detection probability at zero momentum separation with the width inversely proportional to the space-time separation of particle emission points.

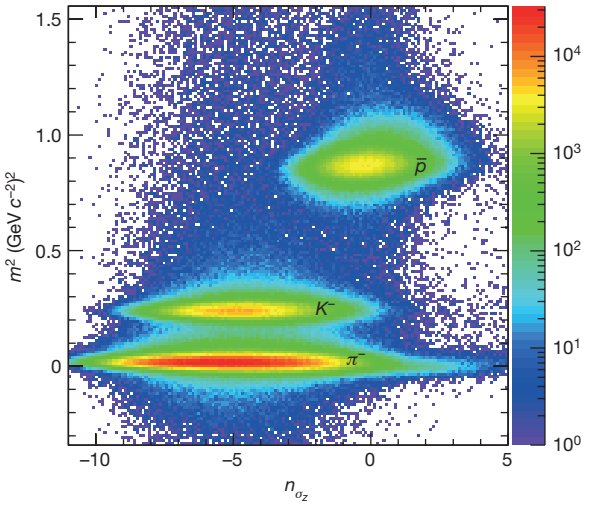

Figure 2 | m^2 versus n_{σ_z} for negatively charged particles. Here $m^2 = (\boldsymbol{p}^2/c^2)(t^2c^2/L^2 - 1)$, where t and L are the time of flight and path length, respectively. c is the light velocity. $z = \ln(\langle dE/dx\rangle/\langle dE/dx\rangle_E)$ and $\langle dE/dx\rangle_E$ is the expected value of $\langle dE/dx\rangle$ for (anti)protons. σ_z is the r.m.s width of the z distribution, and n_{σ_z} is the number of standard deviations from zero, the expected value of z for (anti)protons. The antiprotons, centred at $m^2 = 0.88$ (GeV c^{-2})^2 and $n_{\sigma_z} = 0$, are well separated from other particle species. (Anti)protons satisfying 0.8 (GeV c^{-2})^2 < mass^2 < 1 (GeV c^{-2})^2 and $|n_{\sigma_z}| < 1.5$ are selected for making pairs. With this selection, the purity is >99% for (anti)protons with transverse momentum less than 2 GeV c^{-1}. Colours denote particle population (counts) in cells formed by even division of m^2 and n_{σ_z}.

centrality, based on the observed number of tracks emitted from each collision. Zero per cent centrality corresponds to exactly head-on collisions which produce the most tracks, while 100% centrality corresponds to barely glancing collisions which produce the fewest tracks. The data used here consists of Au + Au collisions at a centre-of-mass energy of 200 GeV per nucleon pair, taken during the operation of RHIC in the year 2011. In total, 500 million events were taken by the minimum-bias trigger at STAR. This trigger selects all particle-producing collisions, regardless of the extent of overlap of the incident nuclei, but with a requirement that collisions must have occurred along the trajectory of the colliding Au ion and within ±30 cm of the centre of STAR's Time Projection Chamber (TPC)[23]. Events used in this analysis correspond to the 30%–80% centrality class, for which the signal due to two-particle interaction is stronger than that from smaller centrality classes, while particle yields are larger than that from larger centrality classes.

The two main detectors used in the measurement are the STAR TPC and the Time of Flight Barrel (TOF)[24]. The TPC is situated in a solenoidal magnetic field (0.5 T), and it provides a three-dimensional image of the ionization trails left along the path of charged particles. The TOF encloses the curved surface of the cylindrical TPC. In conjunction with the momentum measured via the track curvature in TPC, particle identification (PID) is achieved by two key measurements: the mean energy loss per unit track length, $\langle dE/dx\rangle$, which can be used to distinguish particles with different masses or charges, and the time of flight of particles reaching the TOF detector, which can be used, together with tracking information, to derive the square of a particle's mass (m^2). Figure 2 shows a typical calculated mass-squared (m^2) distribution versus n_{σ_z} (see Fig. 2 legend) for antiprotons.

The population distribution of (anti)proton pairs as a function of (anti)proton momentum (k^*) in the pair rest frame (in which the centre of mass of the pair is at rest, convenient for carrying out measurements) is measured for the correlated pairs from within the same event, $A(k^*)$, and, separately, for the non-correlated pairs from two different (mixed) events, $B(k^*)$. The former corresponds to the joint probability $P(\boldsymbol{p}_1, \boldsymbol{p}_2)$, and the latter corresponds to the product of two probabilities, $P(\boldsymbol{p}_1)P(\boldsymbol{p}_2)$, where $P(\boldsymbol{p}_1)$ and $P(\boldsymbol{p}_2)$ each corresponds for observing single (anti)protons. The ratio of the two, $A(k^*)/B(k^*)$, gives the measured CF (see Methods). The observed (anti)protons can come from weak decays of already correlated primary particles, hence introducing residual correlations which contaminate the CF. The dominant contaminations to the CF come from the p–Λ ($\bar{p}$–$\bar{\Lambda}$) and Λ–Λ ($\bar{\Lambda}$–$\bar{\Lambda}$) correlations (where p and Λ denotes the proton and lambda particle, respectively, and $\bar{p}$ and $\bar{\Lambda}$ denotes the corresponding antiparticle), and are taken into account by fitting the CF with corresponding contributions. Taking the two-proton correlation measurement as an example[25],

$$C_{\text{inclusive}}(k^*) = 1 + x_{pp}\left[C_{pp}(k^*; R_{pp}) - 1\right] + x_{p\Lambda}\left[\widetilde{C}_{p\Lambda}(k^*; R_{p\Lambda}) - 1\right] + x_{\Lambda\Lambda}\left[\widetilde{C}_{\Lambda\Lambda}(k^*) - 1\right] \quad (1)$$

where $C_{\text{inclusive}}(k^*)$ is the inclusive CF, and $C_{pp}(k^*; R_{pp})$ is the true proton–proton CF, which can be described by the Lednický and Lyuboshitz analytical model[19]. In this model, for given s-wave scattering parameters, the correlation function with FSI is calculated as the square of the properly symmetrized wavefunction averaged over the total pair spin and the distribution of relative distances of particle emission points in the pair rest frame (see Methods). $\widetilde{C}$ are the residual CFs which are expressed through the p–Λ and Λ–Λ CFs, $C_{p\Lambda}(k^*_{p\Lambda}; R_{p\Lambda})$ and $C_{\Lambda\Lambda}(k^*_{\Lambda\Lambda})$, using integral transformation[25] from $k^*_{p\Lambda}$ and $k^*_{\Lambda\Lambda}$ to k^*_{pp} (see Methods). $C_{p\Lambda}(k^*_{p\Lambda}; R_{p\Lambda})$ is taken from a theoretical calculation[19], which includes all final-state interactions and explains experimental data well[21]. $C_{\Lambda\Lambda}(k^*_{\Lambda\Lambda})$ is from an experimental measurement corrected for

mis-identified Λs (ref. 22). R_{pp} and $R_{p\Lambda}$, assumed to be the same numerically, are the invariant Gaussian radii[21] from the proton–proton correlation and the proton–Λ correlation, respectively. x_{pp}, $x_{p\Lambda}$ and $x_{\Lambda\Lambda}$, taken from the THERMINATOR2 model[26], are the relative contributions from pairs with both daughters from the primary collision, pairs with one daughter from the primary collision and the other one from a Λ decay, and pairs with both daughters from a Λ decay, respectively.

Figure 3 shows the CF for proton–proton pairs (Fig. 3a) and antiproton–antiproton pairs (Fig. 3b), for the 30%–80% centrality class of Au + Au collisions at a centre-of-mass energy of 200 GeV per nucleon pair. The proton–proton CF exhibits a maximum at $k^* \approx 0.02\ \mathrm{GeV}\ c^{-1}$ due to the attractive singlet s-wave interaction between the two detected protons and is consistent with previous measurements[27]. The antiproton–antiproton CF shows a similar structure with the maximum appearing at the same k^* value. In Fig. 3c, the ratio of the inclusive CF for proton–proton pairs to that of antiproton–antiproton pairs is presented. It is well centred at unity for almost all the k^* range, except for the region $k^* < 0.02\ \mathrm{GeV}\ c^{-1}$, where the error becomes large. This indicates that the strong interaction is indistinguishable within errors between proton–proton pairs and antiproton–antiproton pairs. By fitting the CF with equation (1), we determine the singlet s-wave

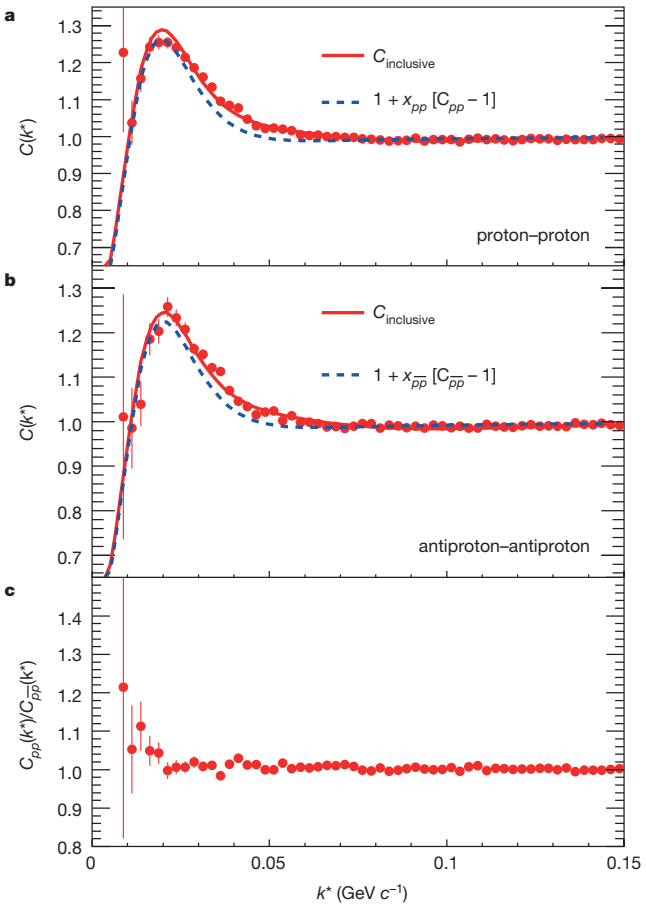

Figure 3 | Correlation functions and their ratio. a, **b**, Correlation functions for proton–proton pairs (**a**) and antiproton–antiproton pairs (**b**). The ratio of the former to the latter is shown in **c**. Errors are statistical only. The fits to the data with equation (1), $C_{\mathrm{inclusive}}(k^*)$, are plotted as solid lines, and the term $1 + x_{pp}[C_{pp}(k^*; R_{pp}) - 1]$ is shown as dashed lines. The χ^2 per number of degrees of freedom of the fit is 1.66 for **a** and 1.61 for **b**. To take advantage of the existing knowledge on the proton–proton interaction, which is relatively well understood, when fitting the proton–proton correlation, f_0 and d_0 for protons are fixed at values measured from proton–proton elastic-scattering experiments, which are 7.82 fm and 2.78 fm, respectively[29]. When fitting the antiproton–antiproton correlation, f_0 and d_0 are treated as free parameters.

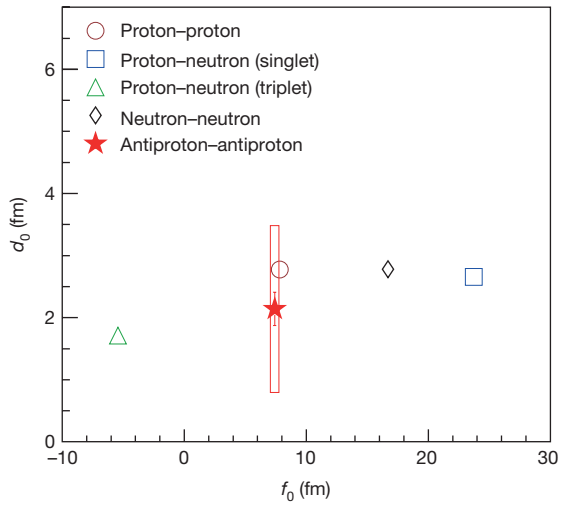

Figure 4 | d_0 versus f_0 for (anti)nucleon-(anti)nucleon interactions. The singlet s-wave scattering length (f_0) and the effective range (d_0) for the antiproton–antiproton interaction (red star) is plotted together with the s-wave scattering parameters for other nucleon–nucleon interactions. Here, statistical errors are represented by error bars, while the horizontal uncertainty for f_0 is smaller than the symbol size, and systematic errors are represented by the box. Errors on other measurements[29,30] are of the order of a few per cent, smaller than the symbol size.

scattering length and effective range for the antiproton–antiproton interaction to be $f_0 = 7.41 \pm 0.19(\mathrm{stat.}) \pm 0.36(\mathrm{sys.})$ fm and $d_0 = 2.14 \pm 0.27(\mathrm{stat.}) \pm 1.34(\mathrm{sys.})$ fm, respectively. Here stat. and sys. indicate statistical and systematic errors, respectively. The extracted radii for protons (R_{pp}) and that for antiprotons ($R_{\bar{p}\bar{p}}$) are $2.75 \pm 0.01(\mathrm{stat.}) \pm 0.04(\mathrm{sys.})$ fm and $2.80 \pm 0.02(\mathrm{stat.}) \pm 0.03(\mathrm{sys.})$ fm, respectively.

Figure 4 presents the first measurement of the antiproton–antiproton interaction, together with prior measurements for nucleon–nucleon interactions. Within errors, the f_0 and d_0 for the antiproton–antiproton interaction are consistent with their antiparticle counterparts—the ones for the proton–proton interaction. Our measurements provide parameterization input for describing the interaction among cold-trapped gases of antimatter ions, as in an ultracold environment, where s-wave scattering dominates and effective-range theory shows that the scattering length and effective range are parameters that suffice to describe elastic collisions. The result provides a quantitative verification of matter–antimatter symmetry in the important and ubiquitous context of the forces responsible for the binding of (anti)nuclei. Possible future improvement of the measurement could be made by reducing the uncertainty from the Λ–Λ CF ($C_{\Lambda\Lambda}(k^*)$), which dominates our systematic error, by further accumulation of data. In addition, a similar extraction of f_0 and d_0 could also be repeated with (anti)proton–(anti)proton CF[28] measured at the Large Hadron Collider, where the yield ratio of antiproton to proton is close to unity.

Online Content Methods, along with any additional Extended Data display items and Source Data, are available in the online version of the paper; references unique to these sections appear only in the online paper.

Received 25 July; accepted 11 September 2015.
Published online 4 November; corrected online 18 November 2015 (see full-text HTML version for details).

1. STAR Collaboration. Observation of the antimatter helium-4 nucleus. *Nature* **473,** 353–356 (2011); erratum **475**, 412 (2011).
2. STAR Collaboration. STAR detector overview. *Nucl. Instrum. Methods Phys. Res. A* **499,** 624–632 (2003).
3. Harrison, M., Ludlam, T. & Ozaki, S. RHIC project overview. *Nucl. Instrum. Methods Phys. Res. A* **499,** 235–244 (2003).
4. Hanbury Brown, R. & Twiss, R. Q. A new type of interferometer for use in radio astronomy. *Phil. Mag.* **45,** 663–682 (1954).
5. Yamazaki, T., Ishikawa, K., Kuramashi, Y. & Ukawa, A. Helium nuclei, deuteron, and dineutron in 2 + 1 flavor lattice QCD. *Phys. Rev. D* **86,** 074514 (2012).
6. Riotto, A. & Trodden, M. Recent progress in baryogenesis. *Annu. Rev. Nucl. Part. Sci.* **49,** 35–75 (1999).

7. Particle Data Group. Olive, K. A. *et al.* Review of particle physics. *Chin. Phys. C* **38,** 090001, 96–106 (2014).
8. Schellekens, M. *et al.* Hanbury Brown Twiss effect for ultracold quantum gases. *Science* **310,** 648–651 (2005).
9. Kiesel, H., Renz, A. & Hasselbach, F. Observation of Hanbury Brown–Twiss anticorrelations for free electrons. *Nature* **418,** 392–394 (2002).
10. Rom, T. *et al.* Free fermion antibunching in a degenerate atomic Fermi gas released from an optical lattice. *Nature* **444,** 733–736 (2006).
11. Goldhaber, G., Goldhaber, S., Lee, W. & Pais, A. Influence of Bose-Einstein statistics on the antiproton-proton annihilation process. *Phys. Rev.* **120,** 300–312 (1960).
12. Kopylov, G. I. & Podgoretskiĭ, M. I. Interference of two-particle states in elementary-particle physics and astronomy. *Sov. Phys. JETP* **42,** 211–214 (1975).
13. Podgoretskiĭ, M. I. Interference correlations of identical pions. Theory. *Sov. J. Part. Nucl.* **20,** 266–282 (1989).
14. Gyulassy, M., Kauffmann, S. K. & Wilson, L. W. Pion interferometry of nuclear collisions. 1. Theory. *Phys. Rev. C* **20,** 2267–2292 (1979).
15. Boal, H. D., Gelbke, C.-K. & Jennings, B. K. Intensity interferometry in subatomic physics. *Rev. Mod. Phys.* **62,** 553–602 (1990).
16. Lednický, R. Correlation femtoscopy of multiparticle processes. *Phys. Atom. Nucl.* **67,** 72–82 (2004).
17. Lisa, M., Pratt, S., Soltz, R. & Wiedemann, U. Femtoscopy in relativistic heavy ion collisions: two decades of progress. *Ann. Rev. Nucl. Part. Sci.* **55,** 357–402 (2005).
18. Koonin, S. E. Proton pictures of high-energy nuclear collisions. *Phys. Lett. B* **70,** 43–47 (1977).
19. Lednický, R. & Lyuboshitz, V. L. Influence of final-state interaction on correlations of two particles with nearly equal momenta. *Sov. J. Nucl. Phys.* **35,** 770–788 (1982).
20. Lednický, R. Notes on correlation femtoscopy. Phys. Atom. Nucl. **71,** 1572–1578 (2008).
21. STAR Collaboration. Proton-Λ correlations in central Au+Au collisions at $\sqrt{s_{NN}}$ = 200 GeV. *Phys. Rev. C* **74,** 064906 (2006).
22. STAR Collaboration. Λ-Λ correlation function in Au+Au collisions at $\sqrt{s_{NN}}$ = 200 GeV. *Phys. Rev. Lett.* **114,** 022301 (2015).
23. Anderson, M. *et al.* The STAR time projection chamber: a unique tool for studying high multiplicity events at RHIC. *Nucl. Instrum. Methods Phys. Res. A* **499,** 659–678 (2003).
24. STAR Collaboration. Multigap RPCs in the STAR experiment at RHIC. *Nucl. Instrum. Methods Phys. Res. A* **661,** S110–S113 (2012).
25. Kisiel, A., Zbroszczyk, H. & Szymański, M. Extracting baryon-antibaryon strong-interaction potentials from $p\overline{\Lambda}$ femtoscopic correlation functions. *Phys. Rev. C* **89,** 054916 (2014).
26. Chojnacki, M., Kisiel, A., Florkowski, W. & Broniowski, W. THERMINATOR 2: THERMal heavy IoN generATOR 2. *Comput. Phys. Commun.* **183,** 746–773 (2012).
27. Pochodzalla, J. *et al.* Two-particle correlations at small relative momenta for ^{40}Ar-induced reactions on ^{197}Au at *E/A* = 60 MeV. *Phys. Rev. C* **35,** 1695–1719 (1987).
28. ALICE Collaboration. One-dimensional pion, kaon, and proton femtoscopy in Pb-Pb collisions at $\sqrt{s_{NN}}$ = 2.76 TeV. Preprint at http://arxiv.org/abs/1506.07884 (2015).
29. Mathelitsch, L. & VerWest, B. J. Effective range parameters in nucleon-nucleon scattering. *Phys. Rev. C* **29,** 739–746 (1984).
30. Šlaus, I., Akaishi, Y. & Tanaka, H. Neutron-neutron effective range parameters. *Phys. Rep.* **173,** 257–300 (1989).

Acknowledgements We thank the RHIC Operations Group and RCF at BNL, the NERSC Center at LBNL, the KISTI Center in Korea, and the Open Science Grid consortium for providing resources and support. This work was supported in part by the Office of Nuclear Physics within the US DOE Office of Science, the US NSF, the Ministry of Education and Science of the Russian Federation, NSFC, the MoST of China (973 Programme No. 2014CB845400), CAS, MoST and MoE of China, the Korean Research Foundation, GA and MSMT of the Czech Republic, FIAS of Germany, DAE, DST and UGC of India, the National Science Centre of Poland, National Research Foundation, the Ministry of Science, Education and Sports of the Republic of Croatia, and RosAtom of Russia.

Author Contributions All authors contributed equally.

Additional Information Reprints and permissions information is available at www.nature.com/reprints. The authors declare no competing financial interests. Readers are welcome to comment on the online version of the paper. Correspondence and requests for materials should be addressed to The STAR Collaboration (star-antiprotonf0d0-l@lists.bnl.gov).

The STAR Collaboration

L. Adamczyk[1], J. K. Adkins[2], G. Agakishiev[3], M. M. Aggarwal[4], Z. Ahammed[5], I. Alekseev[6], J. Alford[7], A. Aparin[3], D. Arkhipkin[8], E. C. Aschenauer[8], G. S. Averichev[3], V. Bairathi[9], A. Banerjee[5], R. Bellwied[10], A. Bhasin[11], A. K. Bhati[4], P. Bhattarai[12], J. Bielcik[13], J. Bielcikova[14], L. C. Bland[8], I. G. Bordyuzhin[6], J. Bouchet[7], J. D. Brandenburg[15], A. V. Brandin[16], I. Bunzarov[3], J. Butterworth[15], H. Caines[17], M. Calderón de la Barca Sánchez[18], J. M. Campbell[19], D. Cebra[18], M. C. Cervantes[20], I. Chakaberia[8], P. Chaloupka[13], Z. Chang[20], S. Chattopadhyay[5], J. H. Chen[21], X. Chen[22], J. Cheng[23], M. Cherney[24], W. Christie[8], G. Contin[25], H. J. Crawford[26], S. Das[27], L. C. De Silva[24], R. R. Debbe[8], T. G. Dedovich[3], J. Deng[28], A. A. Derevschikov[29], B. di Ruzza[8], L. Didenko[8], C. Dilks[30], X. Dong[25], J. L. Drachenberg[31], J. E. Draper[18], C. M. Du[22], L. E. Dunkelberger[32], J. C. Dunlop[8], L. G. Efimov[3], J. Engelage[26], G. Eppley[15], R. Esha[32], O. Evdokimov[33], O. Eyser[8], R. Fatemi[2], S. Fazio[8], P. Federic[14], J. Fedorisin[3], Z. Feng[34], P. Filip[3], Y. Fisyak[8], C. E. Flores[18], L. Fulek[1], C. A. Gagliardi[20], D. Garand[35], F. Geurts[15], A. Gibson[31], M. Girard[36], L. Greiner[25], D. Grosnick[31], D. S. Gunarathne[37], Y. Guo[38], A. Gupta[11], S. Gupta[11], W. Guryn[8], A. Hamad[7], A. Hamed[20], R. Haque[9], J. W. Harris[17], L. He[35], S. Heppelmann[30], S. Heppelmann[8], A. Hirsch[35], G. W. Hoffmann[12], D. J. Hofman[33], S. Horvat[17], B. Huang[33], H. Z. Huang[32], X. Huang[23], P. Huck[34], T. J. Humanic[19], G. Igo[32], W. W. Jacobs[39], H. Jang[40], K. Jiang[38], E. G. Judd[26], S. Kabana[7], D. Kalinkin[6], K. Kang[23], K. Kauder[41], H. W. Ke[8], D. Keane[7], A. Kechechyan[3], Z. H. Khan[33], D. P. Kikoła[36], I. Kisel[42], A. Kisiel[36], S. Klein[25], L. Kochenda[16], D. D. Koetke[31], T. Kollegger[42], L. K. Kosarzewski[36], A. F. Kraishan[37], P. Kravtsov[16], K. Krueger[43], I. Kulakov[42], L. Kumar[4], R. A. Kycia[44], M. A. C. Lamont[8], J. M. Landgraf[8], K. D. Landry[32], J. Lauret[8], A. Lebedev[8], R. Lednicky[3], J. H. Lee[8], X. Li[37], Z. M. Li[34], Y. Li[23], W. Li[21], X. Li[8], C. Li[38], M. A. Lisa[19], F. Liu[34], T. Ljubicic[8], W. J. Llope[41], M. Lomnitz[7], R. S. Longacre[8], X. Luo[34], G. L. Ma[21], R. Ma[8], Y. G. Ma[21], L. Ma[21], N. Magdy[45], R. Majka[17], A. Manion[25], S. Margetis[7], C. Markert[12], H. Masui[25], H. S. Matis[25], D. McDonald[10], K. Meehan[18], N. G. Minaev[29], S. Mioduszewski[20], D. Mishra[9], B. Mohanty[9], M. M. Mondal[20], D. A. Morozov[29], M. K. Mustafa[25], B. K. Nandi[46], Md. Nasim[32], T. K. Nayak[5], G. Nigmatkulov[16], L. V. Nogach[29], S. Y. Noh[40], J. Novak[47], S. B. Nurushev[29], G. Odyniec[25], A. Ogawa[8], K. Oh[48], V. Okorokov[16], D. Olvitt Jr[37], B. S. Page[8], R. Pak[8], Y. X. Pan[32], Y. Pandit[33], Y. Panebratsev[3], B. Pawlik[44], H. Pei[34], C. Perkins[26], A. Peterson[19], P. Pile[8], M. Planinic[49], J. Pluta[36], N. Poljak[49], K. Poniatowska[36], J. Porter[25], M. Posik[37], A. M. Poskanzer[25], J. Putschke[41], H. Qiu[25], A. Quintero[7], S. Ramachandran[2], R. Raniwala[50], S. Raniwala[50], R. L. Ray[12], H. G. Ritter[25], J. B. Roberts[15], O. V. Rogachevskiy[3], J. L. Romero[18], A. Roy[5], L. Ruan[8], J. Rusnak[14], O. Rusnakova[13], N. R. Sahoo[20], P. K. Sahu[27], I. Sakrejda[25], S. Salur[25], J. Sandweiss[17], A. Sarkar[46], J. Schambach[12], R. P. Scharenberg[35], A. M. Schmah[25], W. B. Schmidke[8], N. Schmitz[51], J. Seger[24], P. Seyboth[51], N. Shah[21], E. Shahaliev[3], P. V. Shanmuganathan[7], M. Shao[38], M. K. Sharma[11], B. Sharma[4], W. Q. Shen[21], S. S. Shi[34], Q. Y. Shou[21], E. P. Sichtermann[25], R. Sikora[1], M. Simko[14], M. J. Skoby[39], N. Smirnov[17], D. Smirnov[8], L. Song[10], P. Sorensen[8], H. M. Spinka[43], B. Srivastava[35], T. D. S. Stanislaus[31], M. Stepanov[35], R. Stock[42], M. Strikhanov[16], B. Stringfellow[35], M. Sumbera[14], B. Summa[30], Z. Sun[22], X. M. Sun[34], Y. Sun[38], X. Sun[25], B. Surrow[37], N. Svirida[6], M. A. Szelezniak[25], Z. Tang[38], A. H. Tang[8], T. Tarnowsky[47], A. Tawfik[45], J. H. Thomas[25], A. R. Timmins[10], D. Tlusty[14], M. Tokarev[3], S. Trentalange[32], R. E. Tribble[20], P. Tribedy[5], S. K. Tripathy[27], B. A. Trzeciak[13], O. D. Tsai[32], T. Ullrich[8], D. G. Underwood[43], I. Upsal[19], G. Van Buren[8], G. van Nieuwenhuizen[8], M. Vandenbroucke[37], R. Varma[46], A. N. Vasiliev[29], R. Vertesi[14], F. Videbæk[8], Y. P. Viyogi[5], S. Vokal[3], S. A. Voloshin[41], A. Vossen[39], G. Wang[32], H. Wang[8], J. S. Wang[22], Y. Wang[34], Y. Wang[23], F. Wang[35], J. C. Webb[8], G. Webb[8], L. Wen[32], G. D. Westfall[47], H. Wieman[25], S. W. Wissink[39], R. Witt[52], Y. F. Wu[34], Z. G. Xiao[23], W. Xie[35], K. Xin[15], Y. F. Xu[21], Q. H. Xu[28], H. Xu[22], N. Xu[25], Z. Xu[8], Y. Yang[22], C. Yang[38], S. Yang[38], Y. Yang[34], Q. Yang[38], Z. Ye[33], P. Yepes[15], L. Yi[17], K. Yip[8], I.-K. Yoo[48], N. Yu[34], H. Zbroszczyk[36], W. Zha[38], J. B. Zhang[34], Z. Zhang[21], J. Zhang[28], S. Zhang[21], X. P. Zhang[23], J. Zhang[22], Y. Zhang[38], J. Zhao[34], C. Zhong[21], L. Zhou[38], X. Zhu[23], Y. Zoulkarneeva[3] & M. Zyzak[42]

[1]AGH University of Science and Technology, Cracow 30-059, Poland. [2]University of Kentucky, Lexington, Kentucky, 40506-0055, USA. [3]Joint Institute for Nuclear Research, Dubna, 141 980, Russia. [4]Panjab University, Chandigarh 160014, India. [5]Variable Energy Cyclotron Centre, Kolkata 700064, India. [6]Alikhanov Institute for Theoretical and Experimental Physics, Moscow 117218, Russia. [7]Kent State University, Kent, Ohio 44242, USA. [8]Brookhaven National Laboratory, Upton, New York 11973, USA. [9]National Institute of Science Education and Research, Bhubaneswar 751005, India. [10]University of Houston, Houston, Texas 77204, USA. [11]University of Jammu, Jammu 180001, India. [12]University of Texas, Austin, Texas 78712, USA. [13]Czech Technical University in Prague, FNSPE, Prague, 115 19, Czech Republic. [14]Nuclear Physics Institute AS CR, 250 68 Řež/Prague, Czech Republic. [15]Rice University, Houston, Texas 77251, USA. [16]Moscow Engineering Physics Institute, Moscow 115409, Russia. [17]Yale University, New Haven, Connecticut 06520, USA. [18]University of California, Davis, California 95616, USA. [19]Ohio State University, Columbus, Ohio 43210, USA. [20]Texas A&M University, College Station, Texas 77843, USA. [21]Shanghai Institute of Applied Physics, Shanghai 201800, China. [22]Institute of Modern Physics, Lanzhou 730000, China. [23]Tsinghua University, Beijing 100084, China. [24]Creighton University, Omaha, Nebraska 68178, USA. [25]Lawrence Berkeley National Laboratory, Berkeley, California 94720, USA. [26]University of California, Berkeley, California 94720, USA. [27]Institute of Physics, Bhubaneswar 751005, India. [28]Shandong University, Jinan, Shandong 250100, China. [29]Institute of High Energy Physics, Protvino 142281, Russia. [30]Pennsylvania State University, University Park, Pennsylvania 16802, USA. [31]Valparaiso University, Valparaiso, Indiana 46383, USA. [32]University of California, Los Angeles, California 90095, USA. [33]University of Illinois at Chicago, Chicago, Illinois 60607, USA. [34]Central China Normal University (HZNU), Wuhan 430079, China. [35]Purdue University, West Lafayette, Indiana 47907, USA. [36]Warsaw University of Technology, Warsaw 00-661, Poland. [37]Temple University, Philadelphia, Pennsylvania 19122, USA. [38]University of Science and Technology of China, Hefei 230026, China. [39]Indiana University, Bloomington, Indiana 47408, USA. [40]Korea Institute of Science and Technology Information, Daejeon 305-701, South Korea. [41]Wayne State University, Detroit, Michigan 48201, USA. [42]Frankfurt Institute for Advanced Studies FIAS, Frankfurt 60438, Germany. [43]Argonne National Laboratory, Argonne, Illinois 60439, USA. [44]Institute of Nuclear Physics PAN, Cracow 31-342, Poland. [45]World Laboratory for Cosmology and Particle Physics (WLCAPP), Cairo 11571, Egypt. [46]Indian Institute of Technology, Mumbai 400076, India. [47]Michigan State University, East Lansing, Michigan 48824, USA. [48]Pusan National University, Pusan 609735, South Korea. [49]University of Zagreb, Zagreb, HR-10002, Croatia. [50]University of Rajasthan, Jaipur 302004, India. [51]Max-Planck-Institut fur Physik, Munich 80805, Germany. [52]United States Naval Academy, Annapolis, Maryland 21402, USA.

METHODS

Event mixing for non-correlated pairs and the correction for purity. Non-correlated pairs each consist of two daughter particles. These daughters belong to two events which are carefully chosen so that they have similar event multiplicity and topology. The ratio $A(k^*)/B(k^*)$ (see above), after being normalized at a large k^* (at least 0.25 GeV c^{-1}), gives the measured CF, $C(k^*)_{\mathrm{meas}}$. Because in practice one cannot select 100% pure (anti)protons, a correction to pairs is applied to obtain the PID-purity-corrected CF: $C_{\mathrm{PurityCorrected}}(k^*) = \frac{C_{\mathrm{meas}}(k^*)-1}{\mathrm{PairPurity}(k^*)} + 1$. For simplicity, in equation (1) the subscript "meas" is dropped, and elsewhere in this paper, the subscript "PurityCorrected" is dropped.

The transformation from $k^*_{p\Lambda}$ and $k^*_{\Lambda\Lambda}$ to k^*_{pp}. The residual CF $\widetilde{C}_{p\Lambda}(k^*)$ in equation (1) is naturally expressed as an integral transformation of the parent CF $C_{p\Lambda}(k^*_{p\Lambda})$. Here $k^*_{p\Lambda}$ (and $k^* = k^*_{pp}$) is the magnitude of the three-momentum of either particle in the pair rest frame, while in this case for k^*_{pp}, one of the protons is the decay daughter of Λ. This transformation is done by $\widetilde{C}_{p\Lambda}(k^*_{pp}) = \int C_{p\Lambda}(k^*_{p\Lambda}) T(k^*_{p\Lambda}, k^*_{pp}) \mathrm{d}k^*_{p\Lambda}$, where $T(k^*_{p\Lambda}, k^*_{pp})$ is a matrix that transforms $k^*_{p\Lambda}$ to k^*_{pp} (ref. 25). The transformation matrix is generated with the THERMINATOR2 model[26] which is a Monte Carlo event generator dedicated to studies of the statistical production of particles in relativistic heavy-ion collisions. The same procedure is also used in the transformation from $k^*_{\Lambda\Lambda}$ to k^*_{pp}.

The calculation of the FSI contribution to the correlation function. The femtoscopic correlations due to the Coulomb FSI between the emitted electron and the residual nucleus in beta decay have been well known for more than 80 years; they reveal themselves in a sensitivity of the Fermi function (an analogue of the CF[31]) to the nuclear radius. Compared with non-interacting particles, the FSI effect in a two-particle system with total spin S manifests itself in the substitution of the product of plane waves, $\exp(-ip_1X_a - ip_2X_b)$, by the non-symmetrized Bethe-Salpeter amplitudes $\Psi^{S(-)}_{p_1p_2}(X_a, X_b) = \Psi^{S(+)*}_{p_1p_2}(X_a, X_b)$ (refs 14, 19, 32, 33). For identical particles, the symmetrization requirement in the representation of total pair spin S takes on the same form for both bosons and fermions: the non-symmetrized amplitude should be substituted by $[\Psi^{S(-)}_{p_1p_2}(X_a, X_b) + (-1)^S \Psi^{S(-)}_{p_2p_1}(X_a, X_b)]/\sqrt{2}$. In the pair rest frame, $X_a - X_b = \{t^*, \boldsymbol{r}^*\}$ and $p_1 - p_2 = \{\omega^*_1 - \omega^*_2, 2\boldsymbol{k}^*\}$ where $\omega^*_i = (m_i^2 + k^{*2})^{1/2}$ is the energy of a particle of mass m_i, and t^* and $\boldsymbol{r}^*$ are the relative emission time and relative separation in the pair rest frame, respectively. In this frame, the non-symmetrized Bethe-Salpeter amplitude at equal emission times ($t^* = 0$) reduces, up to an inessential phase factor, to a stationary solution of the scattering problem, $\psi^{S(+)}_{-\boldsymbol{k}^*}(\boldsymbol{r}^*)$. At small relative momenta, $k^* < \sim 1/r^*$, this solution can be used in practical calculations with the condition $|t^*| \ll mr^{*2}$ (refs 19, 32). The equal-time approximation is almost exact in beta decay, and it is usually quite accurate for particles produced in high-energy collisions (to a few per cent in the FSI contribution to CFs of particles even as light as pions[32]). In collisions involving heavy nuclei, the characteristic separation of the emission points, r^*, can be considered substantially larger than the range of the strong-interaction potential. The FSI contribution is then independent of the actual potential form and can be calculated analytically with the help of corresponding scattering amplitudes only[34]. At small k^*, it is basically determined by the s-wave scattering amplitudes $f^S(k^*)$ scaled by the separation r^* (ref. 19).

The analytical calculation of the (anti)proton–(anti)proton correlation function. The (anti)proton–(anti)proton correlation function, $C_{pp}(k^*; R_{pp})$ in equation (1), can be described by the Lednický and Lyuboshitz analytical model[19]. In this model, the correlation function is calculated as the square of the properly symmetrized wavefunction averaged over the total pair spin S and the distribution of relative distances ($\boldsymbol{r}^*$) of particle emission points in the pair rest frame, assuming 1/4 of the singlet and 3/4 of triplet states and a simple Gaussian distribution $\mathrm{d}N/\mathrm{d}^3\boldsymbol{r}^* \approx \exp(-\boldsymbol{r}^{*2}/(4R^2_{pp}))$. Starting with the FSI weight of nucleons emitted with the separation $\boldsymbol{r}^*$ and detected with the relative momentum $\boldsymbol{k}^*$,

$$w(\boldsymbol{k}^*, \boldsymbol{r}^*) = |\psi^{S(+)}_{-\boldsymbol{k}^*}(\boldsymbol{r}^*) + (-1)^S \psi^{S(+)}_{\boldsymbol{k}^*}(\boldsymbol{r}^*)|^2/2$$

where $\psi^{S(+)}_{-\boldsymbol{k}^*}(\boldsymbol{r}^*)$ is the equal-time ($t^* = 0$) reduced Bethe–Salpeter amplitude which can be approximated by the outer solution of the scattering problem[19,35]. This is

$$\psi^{S(+)}_{-\boldsymbol{k}^*}(\boldsymbol{r}^*) = \mathrm{e}^{i\delta_c}\sqrt{A_c(\eta)}\left[\mathrm{e}^{-i\boldsymbol{k}^*\boldsymbol{r}^*}F(-i\eta, 1, i\xi) + f_c(k^*)\frac{\widetilde{G}(\rho,\eta)}{r^*}\right]$$

where $\eta = (k^* a_c)^{-1}$, $a_c = 57.5$ fm is the Bohr radius for two protons, $\rho = k^* r^*$, $\xi = \boldsymbol{k}^*\boldsymbol{r}^* + \rho$, $A_c(\eta)$ is the Coulomb penetration factor given by $A_c(\eta) = 2\pi\eta\,[\exp(2\pi\eta) - 1]^{-1}$, F is the confluent hypergeometric function, $\widetilde{G}(\rho,\eta) = \sqrt{A_c(\eta)}\,[G_0(\rho,\eta) + iF_0(\rho,\eta)]$ is a combination of the regular (F_0) and singular (G_0) s-wave Coulomb functions,

$$f_c(k^*) = \left[\frac{1}{f_0} + \frac{1}{2}d_0k^{*2} - \frac{2}{a_c}h(\eta) - ik^*A_c(\eta)\right]^{-1}$$

is the s-wave scattering amplitude renormalized by the Coulomb interaction, and $h(\eta) = \eta^2\sum_{n=1}^{\infty}[n(n^2+\eta^2)]^{-1} - C - \ln|\eta|$ (here $C \doteq 0.5772$ is the Euler constant). The dependence of the scattering parameters on the total pair spin S is omitted since only the singlet ($S = 0$) s-wave FSI contributes in the case of identical nucleons. The theoretical CF at a given k^* can be calculated as the average FSI weight $\langle w(\boldsymbol{k}^*, \boldsymbol{r}^*)\rangle$ obtained from the separation r^*, simulated according to the Gaussian law, and the angle between the vectors $\boldsymbol{k}^*$ and $\boldsymbol{r}^*$, simulated according to a uniform cosine distribution. This CF is subject to the integral correction[19] $-A_c(\eta)|f_c(k^*)|^2 d_0/(8\sqrt{\pi}R^3_{pp})$ due to the deviation of the outer solution from the true wavefunction in the inner potential region. In addition, in Au + Au collisions the emitting source has a net positive charge, and it influences the CF differently for proton and antiproton pairs. This effect is included in the consideration according to refs 32, 33.

Systematic uncertainties. The systematic uncertainties include variations due to track-wise and pair-wise cuts, the uncertainty in describing the $C_{p\Lambda}$ correlation function[36], and the uncertainty from the $C_{\Lambda\Lambda}$ measurement. The latter dominates the systematic error of d_0 and f_0, and it affects d_0 more than it does f_0 because the shape of the CF is sensitive to d_0, in particular at low k^*. As a consistency check, when fitting the proton–proton CF, both f_0 and d_0 are also allowed to vary freely, and the fitted f_0 and d_0 agree with the results from fitting the antiproton–antiproton CF. Assuming the measurements from different systematic checks follow a uniform distribution, the final systematic error is given by $(\mathrm{maximum} - \mathrm{minimum})/\sqrt{12}$. In our calculations, we consider the two-proton wavefunction, taking into account the Coulomb interaction between point-like protons in all orbital angular momentum waves and the strong interaction in the s-wave only. We neglect the small non-Coulomb electromagnetic contributions due to magnetic interactions, vacuum polarization, and the finite proton size[29,37,38]. This approximation changes the scattering parameters at the level of a few per cent[29,37,38]. The decomposition of systematics from our analysis can be found in Extended Data Table 1.

Sample size. No statistical methods were used to predetermine sample size.

31. Lednický, R. Femtoscopic correlations in multiparticle production and beta-decay. *Braz. J. Phys.* **37,** 939–946 (2007).
32. Lednický, R. Finite-size effect on two-particle production in continuous and discrete spectrum. *Phys. Part. Nucl.* **40,** 307–352 (2009).
33. Erazmus, B. *et al.* Influence of the emitting nucleus on the light-particle correlation function. *Nucl. Phys. A* **583,** 395–400 (1995).
34. Gmitro, M., Kvasil, J., Lednický, R. & Lyuboshitz, V. L. On the sensitivity of nucleon-nucleon correlations to the form of short-range potential. *Czech. J. Phys. B* **36,** 1281–1287 (1986).
35. Landau, L. D. & Lifshitz, E. M. *Kvantovaya Mekhanika: Nerelyativistskaya Teoriya* 3rd edn 585–685 (Nauka, 1974); Landau, L. D. & Lifshitz, E. M. *Quantum Mechanics: Non-relativistic theory* 3rd edn (Pergamon, 2013) [transl.].
36. Bodmer, A. R. & Usmani, Q. N. Coulomb effects and charge symmetry breaking for the $A = 4$ hypernuclei. *Phys. Rev. C* **31,** 1400–1411 (1985).
37. Heller, L. Interaction of two nucleons at low energies. *Rev. Mod. Phys.* **39,** 584–590 (1967).
38. Bergervoet, J. R., van Campen, P. C., van der Sanden, W. A. & de Swart, J. J. Phase shift analysis of 0–30 MeV pp scattering data. *Phys. Rev. C* **38,** 15–50 (1988).

Extended Data Table 1 | The decomposition of systematic errors

	Δf_0 ($\pm$ fm)	Δd_0 ($\pm$ fm)	$\Delta R_{\overline{p}\overline{p}}$ ($\pm$ fm)	ΔR_{pp} ($\pm$ fm)
experimental cuts	0.14	0.33	0.01	0.03
uncertainty of p-Λ CF	0.17	0.19	0.03	0.01
uncertainty of Λ-Λ CF	0.36	1.34	0.03	0.03
THERMINATOR2 model	0.07	0.09	<0.01	<0.01

The table presents systematic uncertainties for f_0 and d_0 for antiproton–antiproton interaction, and R for both proton–proton and antiproton–antiproton interaction. Errors are listed separately by their sources. Assuming the measurements (f_0, d_0 and R) from different systematic checks follow a uniform distribution, the systematic error is given by (maximum measurement − minimum measurement)/$\sqrt{12}$.